


Article

Influence of Grid Resolution and Assimilation Window Size on Simulating Storm Surge Levels

Xin Bi ¹, Wenqi Shi ^{2,*}, Junli Xu ^{1,*} and Xianqing Lv ³ 

¹ School of Mathematics and Physics, Research Institute for Mathematics and Interdisciplinary Sciences, Qingdao University of Science and Technology, Qingdao 266100, China; bixin@mails.qust.edu.cn

² National Marine Environmental Monitoring Center, Ministry of Ecology and Environment, Dalian 116023, China

³ Physical Oceanography Laboratory, Ocean University of China, Qingdao 266100, China; xqinglv@ouc.edu.cn

* Correspondence: wqshi@nmemc.org.cn (W.S.); xjshy1983@163.com (J.X.); Tel.: +86-134-7842-3671 (W.S.); +86-135-1542-6405 (J.X.)

Abstract: Grid resolution and assimilation window size play significant roles in storm surge models. In the Bohai Sea, Yellow Sea, and East China Sea, the influence of grid resolution and assimilation window size on simulating storm surge levels was investigated during Typhoon 7203. In order to employ a more realistic wind stress drag coefficient that varies with time and space, we corrected the storm surge model using the spatial distribution of the wind stress drag coefficient, which was inverted using the data assimilation method based on the linear expression $C_d = (a + b \times U_{10}) \times 10^{-3}$. Initially, two grid resolutions of $5' \times 5'$ and $10' \times 10'$ were applied to the numerical storm surge model and adjoint assimilation model. It was found that the influence of different grid resolutions on the numerical model is almost negligible. But in the adjoint assimilation model, the root mean square (RMS) errors between the simulated and observed storm surge levels under $5' \times 5'$ and $10' \times 10'$ grid resolutions were 11.6 cm and 15.6 cm, and the average PCC and WSS values for 10 tidal stations changed from 89% and 92% in E3 to 93% and 96% in E4, respectively. The results indicate that the finer grid resolution can yield a closer consistency between the simulation and observations. Subsequently, the effects of assimilation window sizes of 6 h, 3 h, 2 h, and 1 h on simulated storm surge levels were evaluated in an adjoint assimilation model with a $5' \times 5'$ grid resolution. The results show that the average RMS errors were 11.6 cm, 10.6 cm, 9.6 cm, and 9.3 cm under four assimilation window sizes. In particular, the RMS errors for the assimilation window sizes of 1 h and 6 h at RuShan station were 3.9 cm and 10.2 cm, a reduction of 61.76%. The PCC and WSS values from RuShan station in E4 and E7 separately showed significant increases, from 85% to 98% and from 92% to 99%. These results demonstrate that when the assimilation window size is smaller, the simulated storm surge level is closer to the observation. Further, the results show that the simulated storm surge levels are closer to the observation when using the wind stress drag coefficient with a finer grid resolution and smaller temporal resolution.

Keywords: grid resolution; assimilation window; numerical model; adjoint assimilation model; storm surge



Citation: Bi, X.; Shi, W.; Xu, J.; Lv, X. Influence of Grid Resolution and Assimilation Window Size on Simulating Storm Surge Levels. *J. Mar. Sci. Eng.* **2024**, *12*, 1233. <https://doi.org/10.3390/jmse12071233>

Academic Editor: Isaac Ginis

Received: 24 May 2024

Revised: 2 July 2024

Accepted: 16 July 2024

Published: 22 July 2024



Copyright: © 2024 by the authors. Licensee MDPI, Basel, Switzerland. This article is an open access article distributed under the terms and conditions of the Creative Commons Attribution (CC BY) license (<https://creativecommons.org/licenses/by/4.0/>).

1. Introduction

A storm surge is an unusual change in sea level induced by tropical cyclones (typhoons, hurricanes) or temperate cyclones (cold tides). For a long time, the damage caused by storm surges has been a major threat to human life, financial status, and infrastructure in coastal areas [1–8]. Southeastern coastal areas in China are often affected by tropical cyclones from the Northwest Pacific Ocean. These disastrous typhoons could bring about serious economic losses and threaten people's lives in low-lying coastal areas [9–15]. The disasters and losses brought by storm surges are difficult to estimate. In 1953, a huge storm surge

caused tremendous disaster in Britain, Germany, the Netherlands, and other European countries, and resulted in thousands of deaths in the Netherlands [1]. In 2005, Hurricane Katrina produced a storm surge level of 4–7 m; at least 1833 individuals were injured or killed and the direct economic loss amounted to USD 108 billion [5]. Therefore, some factors of the storm surge model need to be thoroughly investigated in order to effectively prevent and assess storm surge disasters.

Grid resolution and assimilation window size are two important factors that can affect a storm surge model. In recent years, many scholars have conducted a lot of research on these factors. Jing et al. [16] utilized the Weather Research and Forecasting (WRF) model to explore the large eddy simulation (LES) of the high-wind area near the maximum wind radius of “Tiantu” (2021) using various grid resolutions. They found that altering the grid resolution could significantly affect the local turbulence structure of LES within a limited area, resulting in notable variations in eddy structure and intensity under different grid resolution conditions. Kerr et al. [17] used the Simulating Waves Nearshore (SWAN) model and an Advanced Circulation model (ADCIRC) to simulate the tidal harmonic components and hurricane wave results for Hurricane “Ike” (2008). Their study found that lower resolutions compromised simulation accuracy in coastal areas due to incorrect transmission or lateral attenuation. Moon et al. [18] highlighted that higher-resolution models for complex terrains and coastlines tend to produce higher average surges with a better simulation performance. Dukhovskoy et al. established a storm surge model with high resolution and used it in the Appalachian Gulf in the northeastern Gulf of Mexico during Hurricane Dennis (2005) [19]. Through accurate-resolution simulations of coastal areas and waterways with intricate geometries, they unveiled the unexpected high storm surge processes in this region. Mentaschi et al. [20] developed a wave and storm surge prediction model with high resolution, which exhibited a good predictive ability for both sea level and effective wave height compared with satellite altimeters, tide gauges, and buoys as well as notable improvements compared to previous studies with lower resolutions regarding the reproduction of nearshore dynamics. Garzon et al. [21] found that the North American Mesoscale Forecast System (NAM) and European Center for Medium-Range Weather Forecasts (ECMWF) systems have the highest vertical and horizontal resolution, and indeed displayed the best root mean square deviation (RMSD) and correlation coefficient (CC), while the simulations of water levels based on the weather forecast systems with a higher horizontal resolution obtained better results. Makris et al. [22] used phase-resolving models with a fine resolution for the prediction of average ocean currents at sea level and depth in coastal areas, which are affected by atmospheric forcing and astronomical tides. The results address the significant needs of port authorities, ship pilots, and navigators in battling the problems of vessels impacting the harbor bed during mooring, towage, and berth operations using high-resolution and short-term sea-state forecasting. Fernández-Montblanc et al. [1] designed an unstructured hydrodynamic storm surge and tidal model for Europe. The tidal surge model accounts for the atmospheric pressure, wind, and astronomical tide. It was found that increasing the resolution of atmospheric forcing also improves the predictive ability, most extremely in shallow areas where wind is the main driver of surge production. Mohanty et al. [23] made an attempt to improve the storm surge prediction with a longer lead time using high-resolution mesoscale model outputs. Their findings suggest that the early warnings of tropical cyclones (TCs) obtained by the India Meteorological Department (IMD) should include the surge predictions from these highly reliable mesoscale model products with a 96–72 h lead time in order to mitigate the catastrophic loss associated with storm surges. Based on the research conducted by relevant scholars on grid resolution, it is evident that the effect of grid resolution on simulations of storm surge cannot be disregarded and is an important factor in storm surge simulation.

When analyzing the diurnal variation and hot wave phenomenon of Mars, Zhao et al. introduced different assimilation window lengths into a 4D local ensemble transform Kalman filter (4D-LETKF) to eliminate the artificially caused resonance phenomenon [24]. The study found that the short assimilation window length can effectively eliminate false

resonance. Wang et al. [25] used the ensemble Kalman filter (EnKF) method to compare the influence of assimilating T-TREC-retrieved winds (VTREC) versus radial velocity (V_r) on analyzing and forecasting Typhoon “Qaxi” (2008). The study found that the different assimilation windows had different effects in terms of data assimilation on the inversion wind field and radial wind speed. Zheng et al. [26] used a data assimilation scheme based on the 4DVar method to improve the prediction ability of an existing storm surge model in the North Sea of Germany. By diminishing the assimilation window’s size, they found that the prediction accuracy was enhanced. Based on the ensemble Kalman filter, Kim et al. used a carbon tracker inverse simulation system to study the influence of assimilation window size on the estimation of surface carbon dioxide flux in Asia [27]. The study found that when the assimilation window is shorter, the uncertainty of the optimized surface carbon dioxide flux is greater. DiNapoli et al. [28] applied a preoperative 4-day storm surge ensemble prediction system, called Model for Storm Surge Simulations (M3S), to the southwestern Atlantic continental shelf (SWACS) region. The system assimilated tidal level and elevation data using the four-dimensional ensemble square root filter (4DEnSRF) method. Their study showed that the first 2 days of the 4-day prediction depended on initial conditions, while the last 2 days were influenced by external forcing. Optimal initial conditions were obtained with a 12 h assimilation window size. Khan et al. [29] used numerically efficient hydrodynamics–waves coupled modeling and presented its practical real-time computational set-up; the results show that along this landfalling coastal section, the standard error in the maximum surge level amounts to 2.06, 1.73, and 0.66 m for the T–60 h, T–36 h, and T–12 h forecasts, respectively. Madsen et al. [30] demonstrated the positive impact of coastal altimetry observations when used in a statistical blending method together with tide gauge observations. A positive impact was demonstrated when the blended product was assimilated into a hydrodynamic model of the North Sea and Baltic Sea, showing that the simplified, computational cost-effective assimilation method improves the modeled sea level field. The aforementioned studies suggest that further investigation is warranted to explore the impact of assimilation window size on simulating storm surge levels.

In order to assess the influences of grid resolution and assimilation window size on simulating the storm surge levels, seven experiments were designed in this paper. In order to produce a more realistic wind stress drag coefficient, we have corrected the adjoint assimilation model using a finer grid resolution and smaller assimilation window size. Firstly, we designed four experiments (E1–E4) to examine the influence of different grid resolutions on both the numerical storm surge model and the adjoint assimilation model. Subsequently, we also discussed the impact of assimilation window size on the adjoint assimilation model of storm surges in E4–E7.

This paper consists of four sections. The second section introduces the numerical storm surge model and adjoint assimilation model, as well as the experimental design. A detailed investigation into how the grid resolution and assimilation window size affect the simulated levels of storm surge is provided in the third section. Conclusions are presented in the last part.

2. Materials and Methods

2.1. Typhoon and Stations

Typhoon 7203 formed in the Micronesia region on 5 July 1972 and evolved into a tropical storm on 7 July, peaking early on 11 July. Subsequently, Typhoon 7203 moved northwestward and passed into both the East China Sea and Yellow Sea before making landfall in Tanggu, Tianjin, on 27 July. After traversing Yanshan Mountain, it dissipated at the periphery of the Inner Mongolia Plateau. As a result of its impact, Beijing, Tianjin, Hebei Province, Shandong Province, and the Liaodong Peninsula experienced heavy to torrential rainfall accompanied by winds ranging in force from 9 to 12 as well as strong storm surges in the Bohai Sea. Notably, Qinhuangdao witnessed its highest recorded tidal level at approximately 2.48 m during this event. From 20:00 on 27 July 1972, heavy rainfall

occurred in the jujube forest located in the suburban areas of Beijing. Yanshan’s peculiar topographic features enhance wind convergence, which occurs when horizontal winds cause a net inflow of air into a region (more air entering a vertical column than leaving it). The maximum precipitation recorded within a span of 24 h reached an unprecedented level of 479.2 mm, which has held the record for precipitation in Beijing for a long time. Consequently, mudslides ensued in the mountainous regions of Huairou and Yanqing, resulting in extensive structural damage and claiming approximately 50 lives. In this study, Figure 1 shows the typhoon’s path and the locations of 10 tidal stations, utilized as inputs into the storm surge model. These data are from the typhoon database website (“<http://www.wztf121.com/analyse/wzs>”, accessed on 2 July 2024).

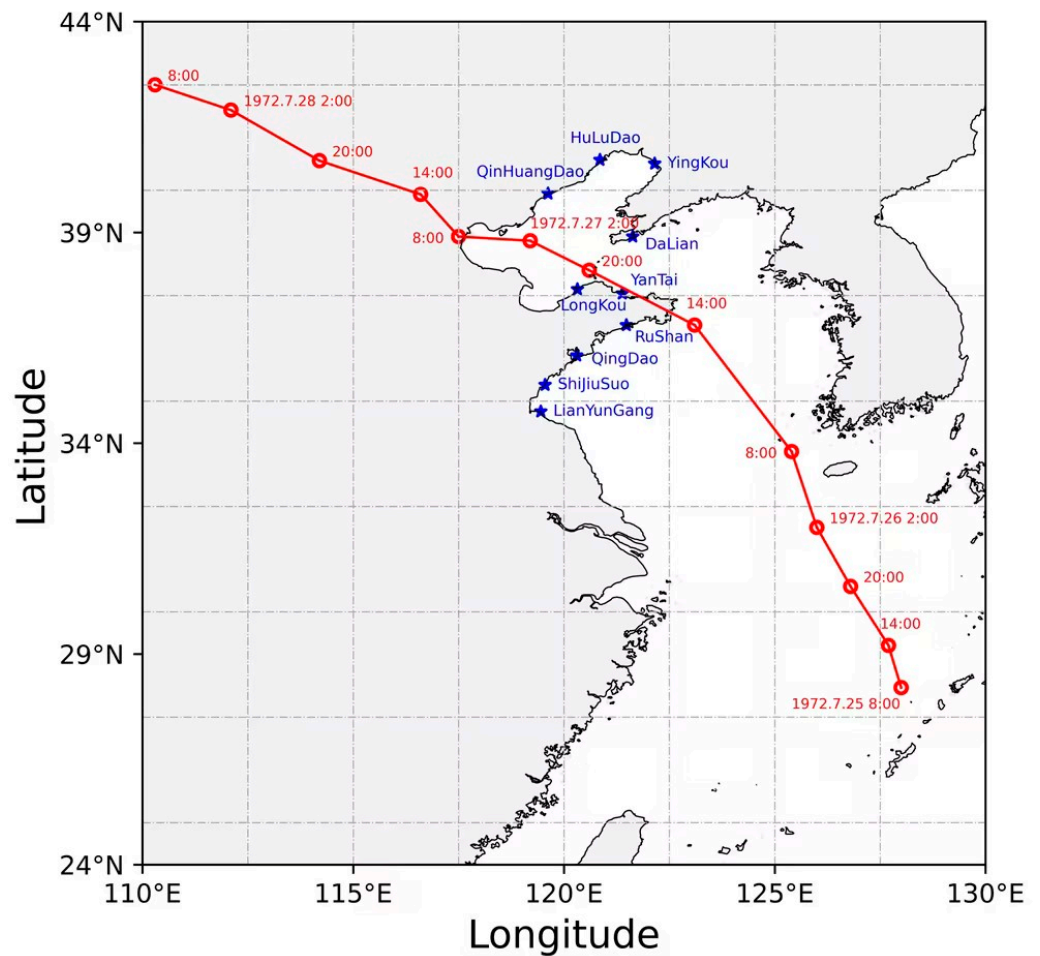


Figure 1. Typhoon path and locations of tidal stations. Star symbols represent the tidal stations’ locations. The solid line indicates the path of Typhoon 7203. Circles represent the time.

2.2. Numerical Storm Surge Model and Adjoint Assimilation Model

In the present study, a depth-averaged shallow-water equation (SWE) model was utilized to calculate the storm surge level. In the Cartesian coordinate system, the primary equations of the storm surge model are composed of the vertically integrated continuum equation and the momentum equation, as follows [31–36]:

$$\frac{\partial \zeta}{\partial t} + \frac{\partial [(h + \zeta)u]}{\partial x} + \frac{\partial [(h + \zeta)v]}{\partial y} = 0 \tag{1}$$

$$\begin{aligned} \frac{\partial u}{\partial t} + u \frac{\partial u}{\partial x} + v \frac{\partial u}{\partial y} - fv + \frac{ku\sqrt{u^2+v^2}}{h+\zeta} - A \left(\frac{\partial^2 u}{\partial x^2} + \frac{\partial^2 u}{\partial y^2} \right) \\ + g \frac{\partial \zeta}{\partial x} + \frac{1}{\rho_\omega} \frac{\partial P_\alpha}{\partial x} - \frac{\rho_\alpha}{\rho_\omega} \frac{C_d W_x \sqrt{W_x^2 + W_y^2}}{h+\zeta} = 0 \end{aligned} \tag{2}$$

$$\begin{aligned} & \frac{\partial v}{\partial t} + u \frac{\partial v}{\partial x} + v \frac{\partial v}{\partial y} + fu + \frac{kv\sqrt{u^2+v^2}}{h+\zeta} - A \left(\frac{\partial^2 v}{\partial x^2} + \frac{\partial^2 v}{\partial y^2} \right) \\ & + g \frac{\partial \zeta}{\partial y} + \frac{1}{\rho_\omega} \frac{\partial P_\alpha}{\partial y} - \frac{\rho_\alpha}{\rho_\omega} \frac{C_d W_y \sqrt{W_x^2 + W_y^2}}{h+\zeta} = 0 \end{aligned} \tag{3}$$

where

- C_d = wind stress drag coefficient;
- ρ_α = air density;
- A = the horizontal eddy viscosity coefficient;
- g = gravitational acceleration;
- t = time;
- u and v = velocity in x and y directions, respectively;
- k = bottom friction factor;
- h = unperturbed water depth;
- W_x and W_y = the surface wind field;
- ρ_ω = sea water density;
- P_α = sea surface pressure;
- x and y = longitude and latitude;
- ζ = surface level;
- f = Coriolis parameter.

Generally speaking, there are some errors in the simulated results caused by approximate assumptions, parameters, etc. In order to decrease the error between the simulated storm surge levels and the observed sea level, we introduced the Lagrange multiplier method and constructed the following form of objective function:

$$J(\zeta) = \frac{1}{2} K_\zeta \int \Sigma (\zeta - \zeta_{obs})^2 dx dy dt \tag{4}$$

where ζ is the simulation, ζ_{obs} is the observation, and K_ζ is the constant.

The corresponding Lagrange function is constructed in the following form:

$$\begin{aligned} L = & J(\zeta) + \int \Sigma \zeta_\alpha \left\{ \frac{\partial \zeta}{\partial t} + \frac{\partial [(h + \zeta)u]}{\partial x} + \frac{\partial [(h + \zeta)v]}{\partial y} \right\} dx dy dt \\ & + \int \Sigma u_\alpha \left[\frac{ku\sqrt{u^2 + v^2}}{h + \zeta} - A \left(\frac{\partial^2 u}{\partial x^2} + \frac{\partial^2 u}{\partial y^2} \right) + \frac{1}{\rho} \frac{\partial P_\alpha}{\partial x} - \frac{\rho_\alpha}{\rho} \frac{C_d W_x \sqrt{W_x^2 + W_y^2}}{h + \zeta} \right] dx dy dt \tag{5} \\ & + \int \Sigma v_\alpha \left[\frac{kv\sqrt{u^2 + v^2}}{h + \zeta} - A \left(\frac{\partial^2 v}{\partial x^2} + \frac{\partial^2 v}{\partial y^2} \right) + \frac{1}{\rho} \frac{\partial P_\alpha}{\partial x} - \frac{\rho_\alpha}{\rho} \frac{C_d W_x \sqrt{W_x^2 + W_y^2}}{h + \zeta} \right] dx dy dt \end{aligned}$$

By means of the derivation approach provided by He et al. [37], the corresponding adjoint equations are achieved:

$$\begin{aligned} & \frac{\partial \zeta_\alpha}{\partial t} + u \frac{\partial \zeta_\alpha}{\partial x} + v \frac{\partial \zeta_\alpha}{\partial y} + \frac{ku\sqrt{u^2+v^2}u_\alpha}{(h+\zeta)^2} + \frac{kv\sqrt{u^2+v^2}v_\alpha}{(h+\zeta)^2} \\ & + g \frac{\partial u_\alpha}{\partial x} + g \frac{\partial v_\alpha}{\partial y} = K_\zeta (\zeta - \zeta_\alpha) \end{aligned} \tag{6}$$

$$\begin{aligned} & \frac{\partial u_\alpha}{\partial t} - \left[f + \frac{kv}{(h+\zeta)\sqrt{u^2+v^2}} \right] v_\alpha - u_\alpha \frac{\partial u}{\partial x} - v_\alpha \frac{\partial v}{\partial x} + \frac{\partial}{\partial x} (uu_\alpha) \\ & + \frac{\partial}{\partial y} (vu_\alpha) + (h + \zeta) \frac{\partial \zeta_\alpha}{\partial x} + A \left(\frac{\partial^2 u_\alpha}{\partial x^2} + \frac{\partial^2 u_\alpha}{\partial y^2} \right) - \frac{k(2u^2+v^2)u_\alpha}{(h+\zeta)\sqrt{u^2+v^2}} = 0 \end{aligned} \tag{7}$$

$$\begin{aligned} & \frac{\partial v_\alpha}{\partial t} - \left[f + \frac{ku}{(h+\zeta)\sqrt{u^2+v^2}} \right] u_\alpha - u_\alpha \frac{\partial u}{\partial y} - v_\alpha \frac{\partial v}{\partial y} + \frac{\partial}{\partial x} (uv_\alpha) \\ & + \frac{\partial}{\partial y} (vv_\alpha) + (h + \zeta) \frac{\partial \zeta_\alpha}{\partial y} + A \left(\frac{\partial^2 v_\alpha}{\partial x^2} + \frac{\partial^2 v_\alpha}{\partial y^2} \right) - \frac{k(u^2+2v^2)v_\alpha}{(h+\zeta)\sqrt{u^2+v^2}} = 0 \end{aligned} \tag{8}$$

where u_α , ζ_α and v_α are the corresponding adjoint variables of ζ , u and v .

The pressure and wind fields used in this model are derived from field observations of meteorological parameters interpolated over the storm surge model grid, based on the work of Jelesnianski et al. [38]. The following is the pressure field:

$$P_\alpha = \begin{cases} P_0 + \frac{1}{4}(P_\infty - P_0)\left(\frac{r}{R}\right)^3, & r \leq R \\ P_\infty - \frac{3}{4}(P_\infty - P_0)\left(\frac{R}{r}\right), & r > R \end{cases} \tag{9}$$

where P_0 is the typhoon’s central pressure, P_α is the sea’s surface pressure at r , and P_∞ is ambient pressure.

The wind field is given by the following:

$$\vec{W} = \begin{cases} \frac{r}{R+r}\left(V_{ox}\vec{i} + V_{oy}\vec{j}\right) + W_R\frac{1}{r}\left(\frac{r}{R}\right)^{\frac{3}{2}}\left(A\vec{i} + B\vec{j}\right), & 0 < r \leq R \\ \frac{R}{R+r}\left(V_{ox}\vec{i} + V_{oy}\vec{j}\right) + W_R\frac{1}{r}\left(\frac{R}{r}\right)^{\frac{1}{2}}\left(A\vec{i} + B\vec{j}\right), & r > R \end{cases} \tag{10}$$

where

R = radius of maximum wind speed W_R ;

V_{ox} and V_{oy} = migration velocities of the typhoon’s center;

\vec{i} and \vec{j} = unit vector in x and y axes;

$A = -[(x - x_c) \sin \theta + (y - y_c) \cos \theta]$;

$B = [(x - x_c) \cos \theta - (y - y_c) \sin \theta]$;

r = distance from grid center (x, y) to typhoon center (x_c, y_c) ;

$\theta = \begin{cases} 20^\circ, & r \leq R \\ 15^\circ, & r > R \end{cases}$

2.3. Experiment and Model

2.3.1. Experimental Design

In order to investigate the effects of grid resolution and assimilation window size on the storm surge level, seven experiments are designed in this section, as presented in Table 1. The wind stress drag coefficient from Wu [39] is used in experiments E1 and E2, with grid resolutions of $10' \times 10'$ and $5' \times 5'$, respectively. In experiments E3 ($10' \times 10'$) and E4 ($5' \times 5'$), the adjoint assimilation method using a linear formula of wind stress drag coefficient is employed to assess the impacts of different grid resolutions on the simulated storm surge levels. The assimilation window size for these two experiments is set as 6 h. In experiments E5, E6, and E7, with a grid resolution of $5' \times 5'$, the assimilation window sizes are adjusted to durations of 3 h, 2 h, and 1 h, respectively. Subsequently, in conjunction with experiment E4, we analyze the influence of assimilation window size on simulating storm surge levels.

Table 1. Seven experiments designed during Typhoon 7203.

| Experiments | Grid Resolution | Assimilation Window |
|-------------|------------------|---------------------|
| E1 | $10' \times 10'$ | × |
| E2 | $5' \times 5'$ | × |
| E3 | $10' \times 10'$ | 6 h |
| E4 | $5' \times 5'$ | 6 h |
| E5 | $5' \times 5'$ | 3 h |
| E6 | $5' \times 5'$ | 2 h |
| E7 | $5' \times 5'$ | 1 h |

2.3.2. Model Setup

In this study, the areas applied in the numerical model and adjoint assimilation model of the storm surge are $110\text{--}130^\circ$ E and $24\text{--}44^\circ$ N, covering the Bohai Sea, Yellow Sea, and

East China Sea. The bottom friction coefficient in those areas is set at a constant of 0.0016. The initial flow velocity and sea surface level are set to 0 in the model. The open boundary conditions are the first island chain and the Taiwan Strait. There is no water flowing in or out of the coastal area on the closed boundary. The bathymetric data are derived from ETOPO1. The barometric pressure and wind stress are taken as the driving forces, and the time interval is 60 s. The model adopts an Arakawa C grid. The observation data used for the experiment are taken from the storm surge levels at 10 tidal stations.

3. Results and Discussion

3.1. Influence of the Grid Resolution on Simulating Storm Surge Levels

The influence of grid resolution on the storm surge level is evaluated using the numerical storm surge model and adjoint assimilation model in this section. Tables 2 and 3 display the RMS errors and absolute mean difference (AMD) errors between simulations and observations at 10 tidal stations in E1–E4 at the end of each stage. However, the results presented in Table 4 are the RMSEs between simulations and observations at each tidal station at the end of the model’s operation. In other words, one in Table 3 is temporal and the other in Table 4 is spatial. It can be seen that the RMS and AMD errors are nearly identical in E1 and E2 using the numerical storm surge model. These results indicate that the influence of grid resolution on the numerical storm surge model is almost negligible.

Table 2. Root mean square errors between simulated and observed levels in E1–E4 (unit: cm).

| Exp | 1 | 2 | 3 | 4 | 5 | 6 | 7 | 8 | 9 | 10 | 11 | 12 * | Mean |
|-----|------|------|------|------|------|------|------|------|------|------|------|------|------|
| E1 | 14.8 | 11.1 | 14.5 | 18.5 | 18.7 | 49.5 | 52.1 | 38.6 | 30.4 | 30.9 | 28.8 | 21.5 | 27.5 |
| E2 | 14.5 | 10.7 | 14.3 | 17.5 | 18.6 | 49.2 | 55.6 | 38.2 | 30.8 | 31.3 | 29.2 | 21.0 | 27.6 |
| E3 | 5.9 | 6.0 | 5.7 | 8.5 | 9.7 | 22.8 | 25.3 | 29.5 | 14.3 | 23.3 | 22.5 | 13.1 | 15.6 |
| E4 | 5.2 | 5.9 | 4.7 | 6.7 | 6.7 | 18.8 | 19.5 | 18.1 | 10.3 | 15.1 | 16.1 | 12.0 | 11.6 |

* The typhoon process selected in this study is 72 h. There are 12 stages during which each stage is set as 6 h in E1–E2. There are also 12 stages during which the assimilation window size is 6 h in E3–E4. These 12 points of comparison in Table 2 represent the average RMSEs between simulations and observations for 10 tidal stations in E1–E4 at the end of each stage.

Table 3. Absolute mean difference errors between simulated and observed levels in E1–E4 (unit: cm).

| Exp | 1 | 2 | 3 | 4 | 5 | 6 | 7 | 8 | 9 | 10 | 11 | 12 * | Mean |
|-----|------|-----|------|------|------|------|------|------|------|------|------|------|------|
| E1 | 12.4 | 8.5 | 11.1 | 15.6 | 16.0 | 42.6 | 45.0 | 33.2 | 27.0 | 26.7 | 24.1 | 18.1 | 23.3 |
| E2 | 12.2 | 8.1 | 11.0 | 14.7 | 15.7 | 41.8 | 49.1 | 33.5 | 27.4 | 26.9 | 24.9 | 17.8 | 23.6 |
| E3 | 4.4 | 4.7 | 4.5 | 6.0 | 7.2 | 16.8 | 19.6 | 23.9 | 10.4 | 19.3 | 19.4 | 9.0 | 12.1 |
| E4 | 4.1 | 4.7 | 3.6 | 4.7 | 4.7 | 11.5 | 16.3 | 15.3 | 8.0 | 11.9 | 13.0 | 8.8 | 8.9 |

* The typhoon process selected in this study is 72 h. There are 12 stages during which each stage is set as 6 h in E1–E2. There are also 12 stages during which the assimilation window size is 6 h in E3–E4. These 12 points of comparison in Table 2 represent the average AMDEs between simulations and observations for 10 tidal stations in E1–E4 at the end of each stage.

The RMS errors in E3 and E4 from the adjoint assimilation model are 15.6 cm and 11.6 cm, and the AMD errors are 12.1 cm and 8.9 cm, respectively. The results reveal that the behavior of the adjoint assimilation model in E4 is better than that in E3, indicating that the finer grid resolution can lead to a closer consistency between simulated and observed storm surge levels. In addition, Table 4 presents the RMS errors, the Pearson correlation coefficient (PCC) [40], and the Willmott skill scores (WSS) [41] between simulation and observation at 10 tidal stations during Typhoon 7203. Taking the Yantai station as an example, the RMS errors in E3 and E4 are 24.5 cm and 18.6 cm, respectively, indicating a reduction of 24.08%. The average RMS errors have decreased by 27.49%, from 17.1 cm in E3 to 12.4 cm in E4. The average PCC values for 10 tidal stations in E1–E4 are 81%, 80%, 89%, and 93%, respectively. The average WSS values in E1–E4 are 82%, 82%, 92%, and 96%. It can be seen that the PCC and WSS values in E1 and E2 are almost identical, while these two indices in E3 and E4

significantly increase; that is, the PCC and WSS in the adjoint assimilation model exceed those in the numerical storm surge model. These results in Tables 3–5 demonstrate that regardless of the values of each RMS error, the PCC, the WSS, or their average values, the finer the grid resolution is, the closer the simulation is to the observation.

Table 4. Root mean square errors (unit: cm), Pearson correlation coefficient, and Willmott skill scores between the simulated and observed storm surge levels in E1–E4 at 10 tidal stations.

| Tidal Stations | E1 | | | E2 | | | E3 | | | E4 | | |
|----------------|------|-----|-----|------|-----|-----|------|-----|-----|------|-----|-----|
| | RMSE | PCC | WSS | RMSE | PCC | WSS | RMSE | PCC | WSS | RMSE | PCC | WSS |
| DaLian | 34.6 | 89% | 71% | 33.8 | 88% | 73% | 25.7 | 88% | 87% | 18.4 | 92% | 93% |
| YingKou | 32.9 | 85% | 89% | 33.6 | 85% | 89% | 14.9 | 97% | 98% | 10.1 | 98% | 99% |
| HuLuDao | 33.9 | 83% | 89% | 34.5 | 82% | 88% | 18.0 | 95% | 97% | 11.9 | 98% | 99% |
| QinHuangDao | 29.7 | 84% | 90% | 30.1 | 83% | 90% | 16.4 | 95% | 97% | 11.3 | 98% | 99% |
| LongKou | 30.0 | 89% | 89% | 30.3 | 89% | 88% | 15.2 | 96% | 97% | 11.9 | 98% | 98% |
| YanTai | 36.9 | 59% | 65% | 36.8 | 59% | 65% | 24.5 | 71% | 82% | 18.6 | 80% | 89% |
| RuShan | 25.9 | 58% | 65% | 27.4 | 57% | 64% | 14.1 | 77% | 84% | 10.2 | 85% | 92% |
| QingDao | 23.2 | 86% | 84% | 24.4 | 86% | 84% | 16.8 | 85% | 88% | 12.2 | 91% | 94% |
| ShiJiuSuo | 23.9 | 89% | 89% | 23.0 | 90% | 90% | 11.6 | 94% | 97% | 9.4 | 96% | 98% |
| LianYunGang | 29.5 | 85% | 86% | 31.1 | 85% | 86% | 13.7 | 93% | 96% | 10.4 | 96% | 98% |
| Mean | 30.0 | 81% | 82% | 30.5 | 80% | 82% | 17.1 | 89% | 92% | 12.4 | 93% | 96% |

Table 5. Root mean square errors and absolute mean difference errors between simulations and observations in E4–E7 (unit: cm).

| Stage * | RMSE | | | | AMDE | | | |
|---------|------|------|------|------|------|------|------|-----|
| | E4 | E5 | E6 | E7 | E4 | E5 | E6 | E7 |
| 1 | 5.2 | 5.2 | 5.1 | 5.5 | 4.1 | 3.5 | 3.1 | 3.2 |
| 2 | 5.9 | 4.7 | 5.1 | 5.0 | 4.7 | 3.6 | 3.0 | 3.0 |
| 3 | 4.7 | 4.2 | 4.5 | 5.3 | 3.6 | 2.8 | 3.1 | 2.7 |
| 4 | 6.7 | 3.8 | 4.4 | 5.7 | 4.7 | 3.1 | 2.8 | 2.5 |
| 5 | 6.7 | 4.2 | 3.5 | 5.1 | 4.7 | 2.7 | 2.4 | 2.7 |
| 6 | 18.8 | 4.9 | 3.7 | 4.7 | 11.5 | 3.2 | 2.9 | 2.4 |
| 7 | 19.5 | 6.1 | 4.3 | 4.7 | 16.3 | 4.1 | 2.9 | 2.4 |
| 8 | 18.1 | 5.3 | 4.6 | 4.9 | 15.3 | 4.3 | 3.0 | 2.5 |
| 9 | 10.3 | 4.6 | 4.9 | 4.0 | 8.0 | 3.7 | 2.9 | 2.5 |
| 10 | 15.1 | 6.8 | 5.7 | 3.1 | 11.9 | 5.3 | 3.6 | 2.4 |
| 11 | 16.1 | 17.5 | 5.8 | 3.3 | 13.0 | 11.4 | 4.4 | 2.5 |
| 12 | 12.0 | 20.4 | 5.7 | 3.4 | 8.8 | 11.1 | 4.2 | 2.5 |
| 13 | | 18.5 | 4.3 | 4.0 | | 14.6 | 3.5 | 3.1 |
| 14 | | 17.1 | 5.6 | 4.3 | | 13.5 | 4.5 | 2.5 |
| 15 | | 22.1 | 7.6 | 5.0 | | 18.0 | 6.2 | 2.5 |
| 16 | | 16.5 | 13.1 | 5.1 | | 12.4 | 9.1 | 2.6 |
| 17 | | 12.3 | 18.2 | 5.1 | | 9.4 | 14.4 | 2.7 |
| 18 | | 12.2 | 18.6 | 5.2 | | 8.0 | 15.1 | 2.7 |
| 19 | | 14.4 | 19.1 | 5.8 | | 11.3 | 14.8 | 3.3 |
| 20 | | 11.1 | 18.8 | 5.9 | | 8.8 | 13.9 | 3.7 |
| 21 | | 10.1 | 15.3 | 6.3 | | 7.6 | 11.9 | 4.6 |
| 22 | | 10.7 | 19.8 | 6.4 | | 6.9 | 15.8 | 4.8 |
| 23 | | 12.6 | 14.5 | 6.4 | | 9.4 | 10.3 | 4.9 |
| 24 | | 7.9 | 12.4 | 5.4 | | 4.8 | 8.9 | 3.9 |
| 25 | | | 10.5 | 5.1 | | | 6.6 | 4.0 |
| 26 | | | 11.0 | 3.9 | | | 7.5 | 2.8 |
| 27 | | | 10.8 | 4.8 | | | 7.8 | 3.7 |
| 28 | | | 11.0 | 5.9 | | | 7.7 | 4.9 |
| 29 | | | 9.8 | 7.2 | | | 6.6 | 6.2 |
| 30 | | | 11.0 | 8.1 | | | 8.6 | 6.3 |
| 31 | | | 10.2 | 11.0 | | | 8.2 | 7.5 |

Table 5. Cont.

| Stage * | RMSE | | | | AMDE | | | |
|---------|------|------|------|------|------|-----|-----|------|
| | E4 | E5 | E6 | E7 | E4 | E5 | E6 | E7 |
| 32 | | | 9.8 | 16.1 | | | 6.7 | 10.8 |
| 33 | | | 9.7 | 16.4 | | | 5.5 | 13.3 |
| 34 | | | 10.0 | 17.3 | | | 6.3 | 13.4 |
| 35 | | | 8.4 | 16.1 | | | 6.6 | 13.0 |
| 36 | | | 7.6 | 21.6 | | | 5.3 | 18.2 |
| 37 | | | | 18.6 | | | | 15.1 |
| 38 | | | | 19.6 | | | | 14.4 |
| 39 | | | | 19.0 | | | | 12.7 |
| 40 | | | | 18.8 | | | | 13.7 |
| 41 | | | | 16.5 | | | | 11.8 |
| 42 | | | | 14.9 | | | | 11.5 |
| 43 | | | | 18.6 | | | | 14.9 |
| 44 | | | | 19.1 | | | | 14.9 |
| 45 | | | | 15.6 | | | | 11.2 |
| 46 | | | | 12.6 | | | | 8.2 |
| 47 | | | | 12.9 | | | | 9.2 |
| 48 | | | | 11.6 | | | | 8.2 |
| 49 | | | | 9.1 | | | | 6.7 |
| 50 | | | | 9.7 | | | | 6.6 |
| 51 | | | | 9.9 | | | | 6.7 |
| 52 | | | | 11.2 | | | | 8.0 |
| 53 | | | | 10.0 | | | | 6.5 |
| 54 | | | | 9.9 | | | | 5.9 |
| 55 | | | | 10.4 | | | | 6.4 |
| 56 | | | | 10.2 | | | | 5.7 |
| 57 | | | | 9.1 | | | | 5.4 |
| 58 | | | | 8.6 | | | | 5.6 |
| 59 | | | | 9.6 | | | | 7.2 |
| 60 | | | | 9.4 | | | | 7.2 |
| 61 | | | | 8.9 | | | | 6.9 |
| 62 | | | | 8.6 | | | | 6.5 |
| 63 | | | | 8.8 | | | | 6.5 |
| 64 | | | | 10.1 | | | | 6.4 |
| 65 | | | | 9.4 | | | | 5.4 |
| 66 | | | | 10.0 | | | | 5.2 |
| 67 | | | | 10.5 | | | | 6.1 |
| 68 | | | | 8.5 | | | | 4.8 |
| 69 | | | | 9.7 | | | | 6.8 |
| 70 | | | | 6.7 | | | | 5.4 |
| 71 | | | | 4.4 | | | | 3.6 |
| 72 | | | | 7.0 | | | | 4.8 |
| Mean | 11.6 | 10.6 | 9.6 | 9.3 | 8.9 | 7.7 | 6.9 | 6.5 |

* The typhoon process selected in this study lasts 72 h. In stages 12, 24, 36, and 72, the assimilation window sizes are 6, 3, 2, and 1 h in E4–E7. The 12, 24, 36, and 72 points of comparison in Table 5 represent the RMSEs and AMDEs between simulations and observations in E4–E7 at the end of each stage.

The storm surge levels and the differences between simulated and observed levels at Yingkou, Huludao, and Yantai tidal stations in E1–E4 are depicted in Figures 2–4. In E3–E4, the storm surge levels are simulated via the spatial distribution of the wind stress drag coefficient, which is inverted via the data assimilation method based on the linear expression $C_d = (a + b \times U_{10}) \times 10^{-3}$. According to the time series graphs of simulations and observations, it is apparent that the results from E1 and E2 are largely different from the observed levels, and the simulations of storm surge levels in E3 and E4 more closely approach the observed values. This result shows that the adjoint assimilation model is superior to the numerical storm surge model. At the same time, comparing the results of E3 and E4, it can be found that the result in E4 is slightly superior to that in E3, showing

that simulating storm surge levels with finer grid resolutions yields results that are closer to the observations.

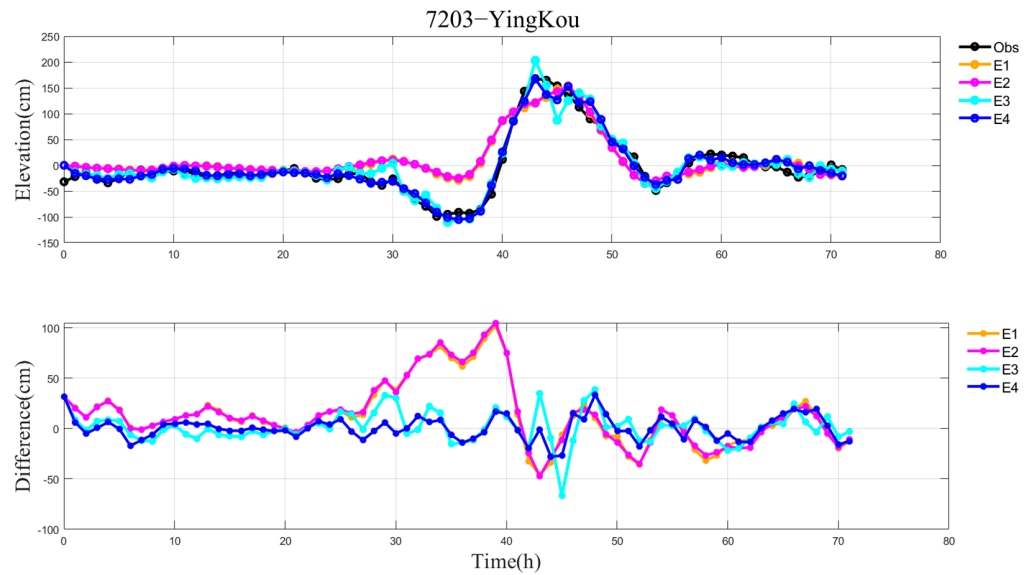


Figure 2. Simulated storm surge levels in E1–E4 and the observed level (**top**), and the differences between the simulation and observation (**bottom**) at YingKou station during Typhoon 7203.

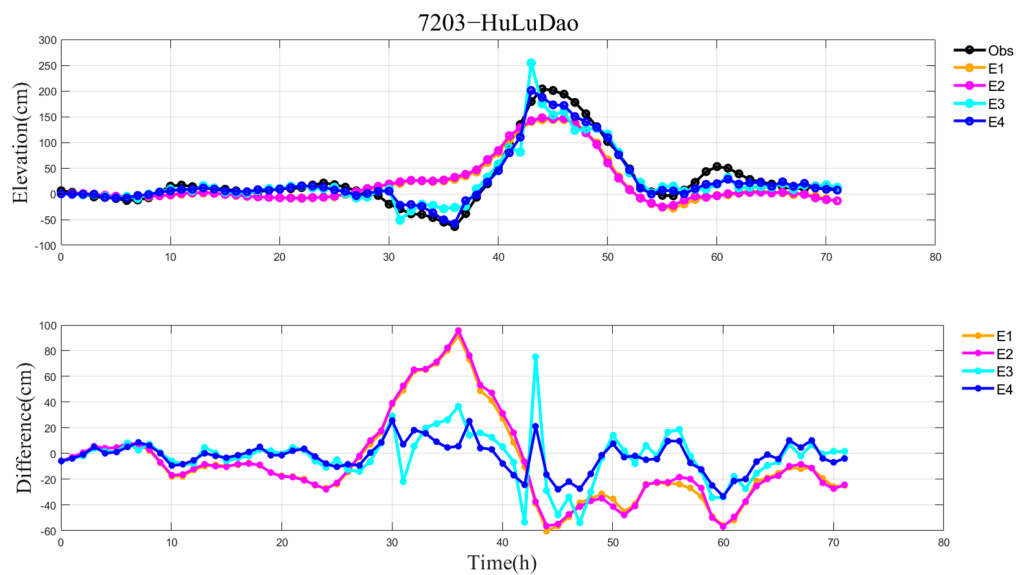


Figure 3. Simulated storm surge levels in E1–E4 and the observed level (**top**), and the differences between the simulation and observation (**bottom**) at HuLuDao station during Typhoon 7203.

The peak values of the storm surge level between the simulations and observations in E1–E4 are exhibited in Figure 5. At YingKou station, the simulated peaks of storm surge levels in E1, E2, and E4 were, respectively, underestimated by 46.35 cm, 47.69 cm, and 0.74 cm, and the peak in E3 was overestimated by 34.3 cm compared to the observed peak surge. Similarly, at HuLuDao station, the peaks of surges in E1–E4 were underestimated by 60.17 cm, 56.17 cm, 28.4 cm, and 16.4 cm compared to the observation, respectively. The simulated peaks of surge in E3 and E4 approached more closely to the observations than those in E1 and E2, indicating that the adjoint assimilation model performs better than the numerical model. Meanwhile, the peak simulated in E4 is closer to the observation than that in E3, indicating that a finer grid resolution can result in better simulation results.

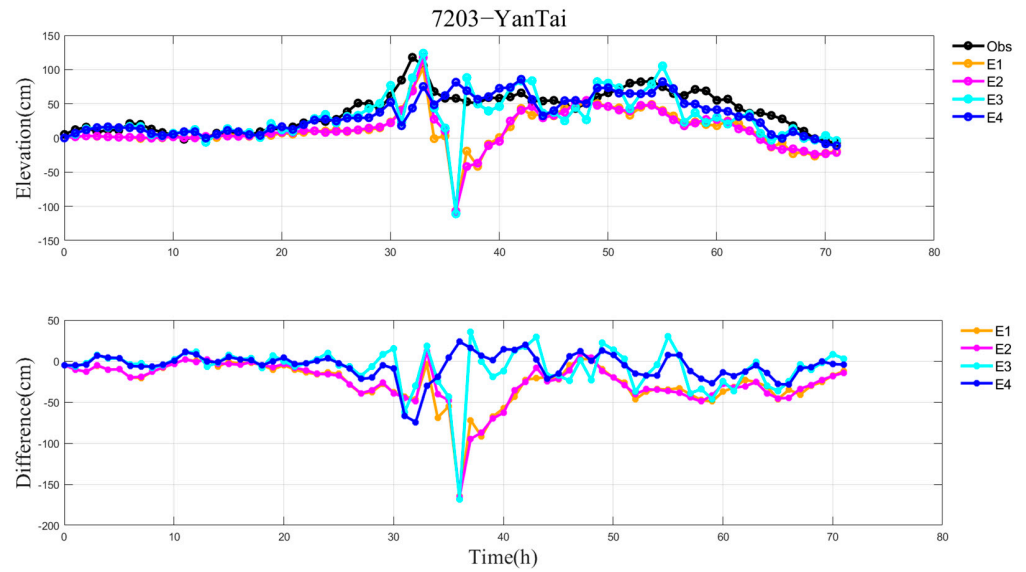


Figure 4. Simulated storm surge levels in E1–E4 and the observed level (**top**), and the differences between the simulation and observation (**bottom**) at YanTai station during Typhoon 7203.

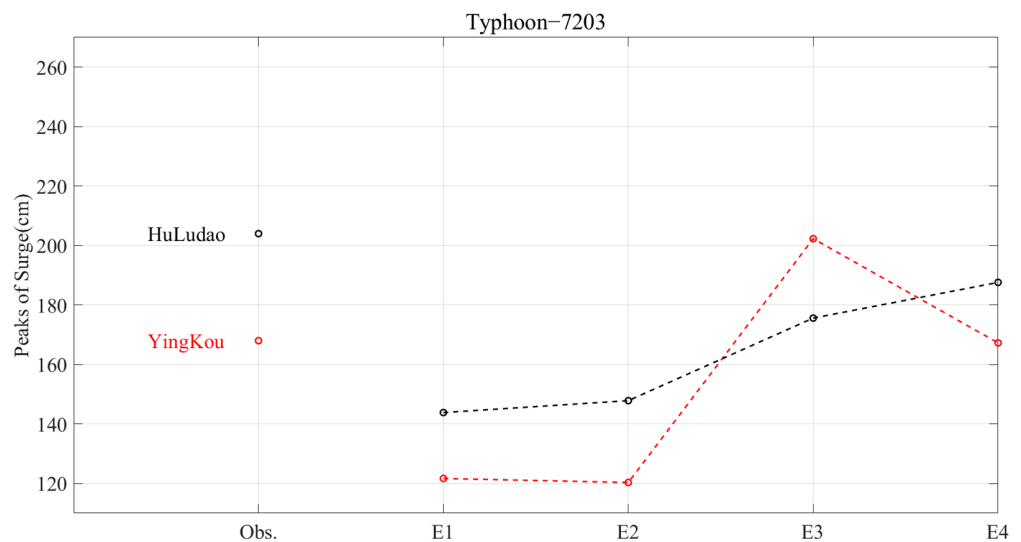


Figure 5. Peaks of simulated and observed storm surge levels in E1–E4 at HuLuDao and YingKou stations.

3.2. Influence of Assimilation Window Size on Simulated Storm Surge Levels

The influence of the assimilation window size on the simulated levels of storm surge is addressed by setting 6 h, 3 h, 2 h, and 1 h sizes under a grid resolution of $5' \times 5'$. The RMS errors and AMD errors between the simulations and observations in E4–E7 are listed in Table 5. The RMS errors in E4–E7 are, on average, 11.6 cm, 10.6 cm, 9.6 cm, and 9.3 cm, respectively, and the mean RMS errors in E5, E6, and E7 are 8.62%, 17.24%, and 19.83% lower when compared to that in E4. Additionally, the RMS errors, the PCC, the WSS between the simulations and observations at 10 tidal stations, and their averages in E4–E7 at 10 tidal stations are listed in Table 6. Taking RuShan station as an example, the RMS errors in E4–E7 are 10.2 cm, 7.7 cm, 6.1 cm, and 3.9 cm, respectively. The RMS errors in E5, E6, and E7 are 24.51%, 40.20%, and 61.76% lower when compared with that in E4. The average PCC values for 10 tidal stations in E4–E7 are 93%, 95%, 97%, and 97%, respectively. The average WSS values in E4–E7 are 96%, 97%, 98%, and 98%. These two evaluation indicators increase as the assimilation window size gradually decreases, and the accuracy of the storm surge models in E6 and E7 shows little difference. The above results indicate that the simulations of storm surge levels are closer to the observed levels when the assimilation

window size is smaller. Via comprehensive comparison, we can see that the assimilation window size of 1 h or 2 h is applicable in the adjoint assimilation model of storm surge when simulating storm surge levels.

Table 6. Root mean square errors (unit: cm), Pearson correlation coefficient, and Willmott skill scores between the simulated storm surge levels and observations in E4–E7 at 10 tidal stations.

| Tidal Stations | E4 | | | E5 | | | E6 | | | E7 | | |
|----------------|------|-----|-----|------|-----|-----|------|-----|-----|------|-----|-----|
| | RMSE | PCC | WSS | RMSE | PCC | WSS | RMSE | PCC | WSS | RMSE | PCC | WSS |
| DaLian | 18.4 | 92% | 93% | 18.8 | 94% | 93% | 17.9 | 95% | 93% | 18.6 | 96% | 93% |
| YingKou | 10.1 | 98% | 99% | 10.4 | 98% | 99% | 6.9 | 99% | 99% | 4.7 | 99% | 99% |
| HuLuDao | 11.9 | 98% | 99% | 10.1 | 99% | 99% | 10.8 | 98% | 99% | 10.2 | 99% | 99% |
| QinHuangDao | 11.3 | 98% | 99% | 10.4 | 98% | 99% | 11.2 | 98% | 99% | 10.5 | 98% | 99% |
| LongKou | 11.9 | 98% | 98% | 6.3 | 99% | 99% | 5.6 | 99% | 99% | 5.0 | 99% | 99% |
| YanTai | 18.6 | 80% | 89% | 17.8 | 85% | 91% | 7.2 | 97% | 98% | 9.0 | 95% | 97% |
| RuShan | 10.2 | 85% | 92% | 7.7 | 91% | 95% | 6.1 | 94% | 97% | 3.9 | 98% | 99% |
| QingDao | 12.2 | 91% | 94% | 11.1 | 94% | 95% | 11.1 | 95% | 96% | 10.3 | 96% | 97% |
| ShiJiuSuo | 9.4 | 96% | 98% | 12.4 | 95% | 96% | 14.4 | 95% | 96% | 14.9 | 95% | 95% |
| LianYunGang | 10.4 | 96% | 98% | 8.4 | 98% | 99% | 9.9 | 97% | 98% | 8.3 | 98% | 99% |
| Mean | 12.4 | 93% | 96% | 11.3 | 95% | 97% | 10.1 | 97% | 98% | 9.5 | 97% | 98% |

The storm surge levels and the differences between simulations and observations at YingKou, LongKou, and RuShan tidal stations in E4–E7 are depicted in Figures 6–8. In particular, at RuShan station, the PCC and WSS values in E4 and E7 show significant increases from 85% to 98% and from 92% to 99%, respectively. Comparatively, the simulated values in E4 and E5 are far from the observed values, and the simulated values in E6 and E7 are closer to the observations. These findings all suggest that the storm surge levels simulated with smaller assimilation window sizes are closer to the observed levels.

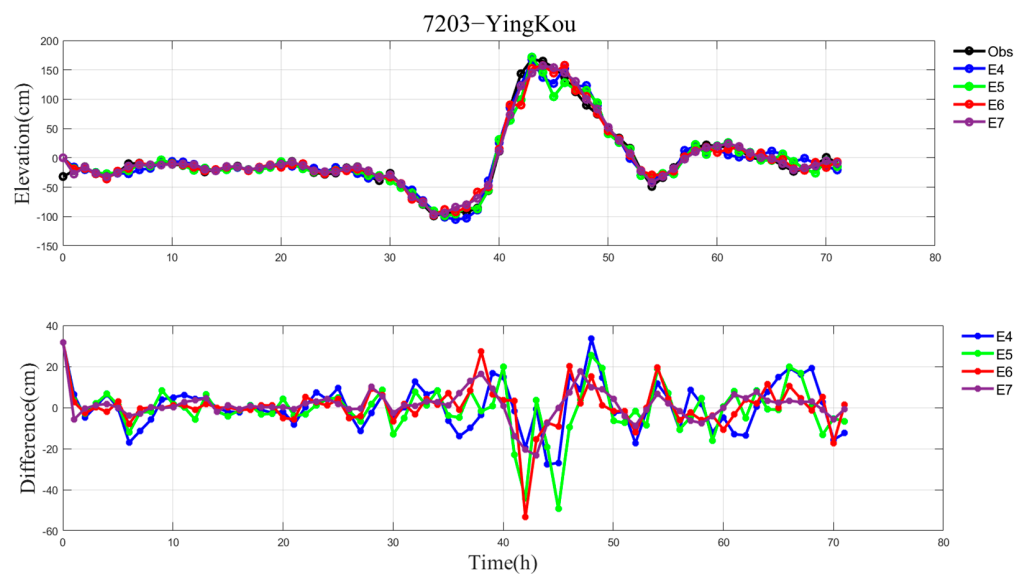


Figure 6. Simulated storm surge levels in E4–E7 and observed level (top), and the differences between the simulation and observation (bottom) at YingKou station during Typhoon 7203.

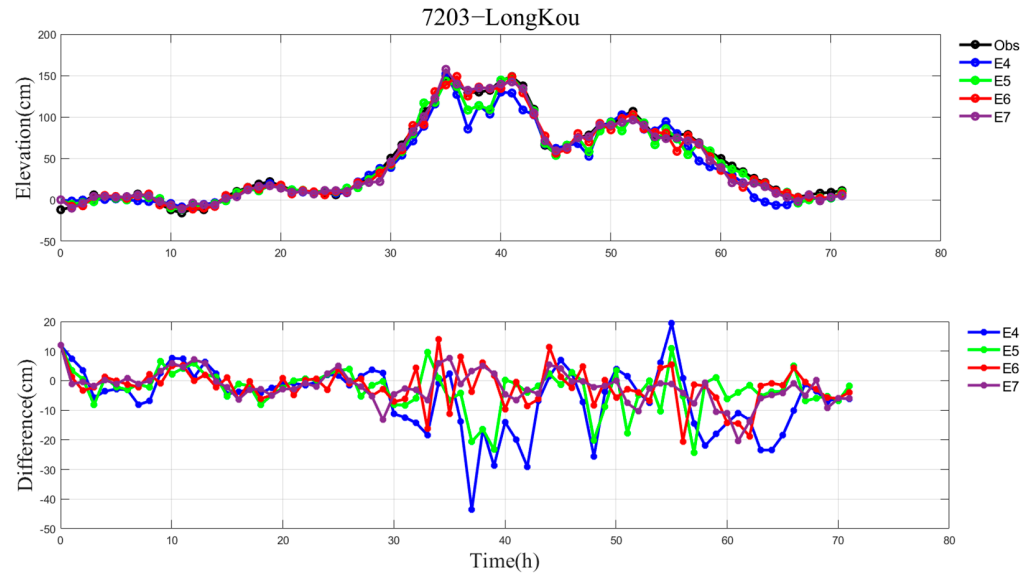


Figure 7. Simulated storm surge levels in E4–E7 and observed level (top), and the differences between the simulation and observation (bottom) at LongKou station during Typhoon 7203.

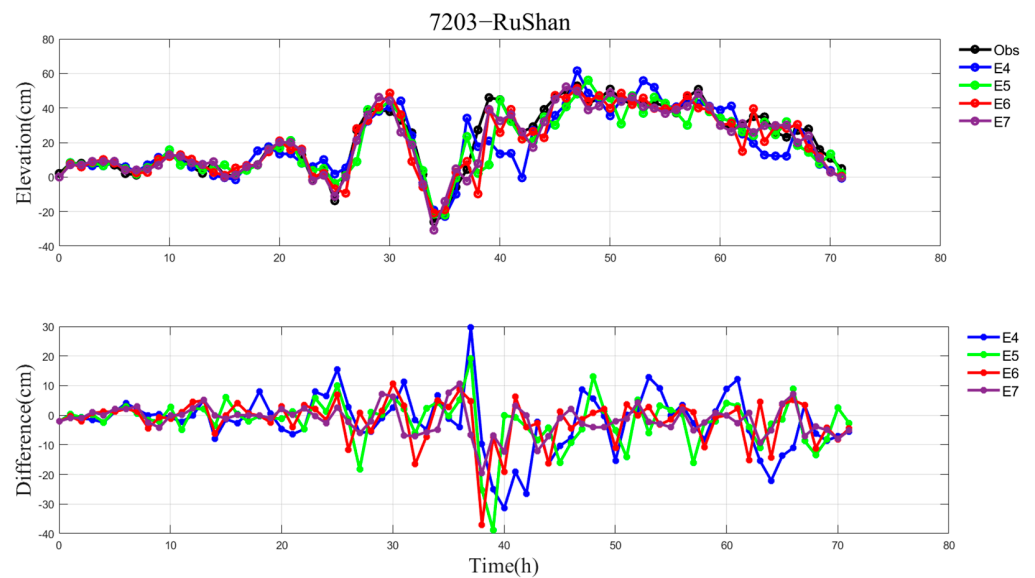


Figure 8. Simulated storm surge levels in E4–E7 and observed level (top), and the differences between the simulation and observation (bottom) at RuShan station during Typhoon 7203.

4. Conclusions

In relation to Typhoon 7203, we have explored the effects of the grid resolution and assimilation window size on simulations of storm surge levels in the Bohai Sea, Yellow Sea, and East China Sea in this paper. In the adjoint assimilation model, we used the inverted spatial distribution of the wind stress drag coefficient to calculate the storm surge level via the data assimilation method based on the linear expression $C_d = (a + b \times U_{10}) \times 10^{-3}$.

In order to investigate the influences of different grid resolutions on simulations of storm surge levels, we conducted four experiments. In E1 and E2, two grid resolutions of $10' \times 10'$ and $5' \times 5'$ were set up in the numerical storm surge model. Similarly, two experiments were carried out on the adjoint assimilation method using grid resolutions of $10' \times 10'$ and $5' \times 5'$ in E3 and E4. The results of the evaluation indicators, comprising the values of RMS error, AMD error, PCC, WSS, and their average, reveal that in E1 and E2, the impact of the grid resolution was minimal and practically negligible in the numerical model of storm surges. However, in E3 and E4, when using the adjoint assimilation model,

varying grid resolutions were found to significantly affect the simulation accuracy. It was found that finer grids can yield more precise simulation levels.

The influence of the assimilation window's size on simulations of storm surge levels with a $5' \times 5'$ grid resolution was investigated in the present study. Using the adjoint assimilation method in E4–E7, assimilation window sizes with intervals of 6 h, 3 h, 2 h, and 1 h were assessed, respectively. The results demonstrate that the performance in E6 and E7 was superior to that in E4 and E5, as suggested by the comparison of RMS error, AMD error, PCC, and WSS. In particular, the average PCC and WSS values reached 97% and 98% when the assimilation window sizes were 2 h and 1 h in E6–E7. Therefore, the effect of assimilation window size on storm surge levels is also very important. Smaller assimilation window size showed enhanced accuracy and higher PCC and WSS in simulating storm surge levels.

In addition to the grid resolution and assimilation window size, there are many other factors that can also affect the storm surge model, such as the bottom friction coefficient, the time interval of external forcing, the type of external forcing, and the wind stress drag coefficient. In future research, we will consider the effects of these factors on model performance.

Author Contributions: Conceptualization, W.S.; methodology, W.S. and X.B.; software, X.B. and J.X.; formal analysis, J.X.; writing—original draft preparation, X.B.; writing—review and editing, J.X. and X.L.; supervision, X.L.; funding acquisition, W.S. All authors have read and agreed to the published version of the manuscript.

Funding: This research was funded by the National Natural Science Foundation of China, grant numbers 41606006 and 41806219.

Institutional Review Board Statement: Not applicable.

Informed Consent Statement: Not applicable.

Data Availability Statement: Typhoon 7203 data used in this paper was collected from the Wenzhou Typhoon Network, this data can be found here: <http://www.wztf121.com/> (accessed on 2 July 2024).

Conflicts of Interest: The authors declare no conflicts of interest.

References

1. Fernández-Montblanc, T.; Vousdoukas, M.I.; Ciavola, P.; Voukouvalas, E.; Mentaschi, L.; Breyiannis, G.; Feyen, L.; Salamon, P. Towards robust pan-European storm surge forecasting. *Ocean Modell.* **2019**, *133*, 129–144. [[CrossRef](#)]
2. Yang, Z.Q.; Wang, T.P.; Castrucci, L.; Miller, I. Modeling assessment of storm surge in the Salish Sea. *Estuar. Coast. Shelf Sci.* **2020**, *238*, 106552. [[CrossRef](#)]
3. Yin, C.T.; Zhang, W.S.; Xiong, M.J.; Wang, J.H.; Zhou, C.Y.; Dou, X.P.; Zhang, J.S. Storm surge responses to the representative tracks and storm timing in the Yangtze Estuary, China. *Ocean Eng.* **2021**, *233*, 109020. [[CrossRef](#)]
4. Familkhalili, R.; Talke, S.A.; Jay, D.A. Tide-Storm Surge Interactions in Highly Altered Estuaries: How Channel Deepening Increases Surge Vulnerability. *J. Geophys. Res. Oceans* **2020**, *125*, e2019JC015286. [[CrossRef](#)]
5. Qin, Y.; Su, C.Y.; Chu, D.D.; Zhang, J.C.; Song, J.B. A Review of Application of Machine Learning in Storm Surge Problems. *J. Mar. Sci. Eng.* **2023**, *11*, 1729. [[CrossRef](#)]
6. Chen, B.R.; He, J.Y.; He, Z.G.; Li, L.; Chen, Q.; Li, F.X.; Chu, D.D.; Cao, Z.; Yang, X.C. Potential impacts of storm surge-induced flooding based on refined exposure estimation: A case study in Zhoushan island, China. *Geomat. Nat. Hazards Risk* **2023**, *14*, 2232080. [[CrossRef](#)]
7. Tan, Y.C.; Zhang, W.; Feng, X.B.; Guo, Y.P.; Hoitink, A.J.F. Storm surge variability and prediction from ENSO and tropical cyclones. *Environ. Res. Lett.* **2023**, *18*, 024016. [[CrossRef](#)]
8. Toyoda, M.; Fukui, N.; Miyashita, T.; Shimura, T.; Mori, N. Uncertainty of storm surge forecast using integrated atmospheric and storm surge model: A case study on Typhoon Haishen 2020. *Coast. Eng. J.* **2022**, *64*, 135–150. [[CrossRef](#)]
9. Chu, D.D.; Zhang, J.C.; Wu, Y.S.; Jiao, X.H.; Qian, S.H. Sensitivities of modelling storm surge to bottom friction, wind drag coefficient, and meteorological product in the East China Sea. *Estuar. Coast. Shelf Sci.* **2019**, *231*, 106460. [[CrossRef](#)]
10. Du, M.; Hou, Y.J.; Hu, P.; Wang, K. Effects of typhoon paths on storm surge and coastal inundation in the Pearl River Estuary, China. *Remote Sens.* **2020**, *12*, 1851. [[CrossRef](#)]
11. Guo, Y.X.; Hou, Y.J.; Liu, Z.; Du, M. Risk prediction of coastal hazards induced by typhoon: A case study in the coastal region of Shenzhen, China. *Remote Sens.* **2020**, *12*, 1731. [[CrossRef](#)]
12. Chen, W.B.; Chen, H.; Hisao, S.C.; Chang, C.H.; Lin, L.Y. Wind forcing effect on hindcasting of typhoon-driven extreme waves. *Ocean Eng.* **2019**, *188*, 106260. [[CrossRef](#)]

13. Hisao, S.C.; Chen, H.; Wu, H.L.; Chen, W.B.; Chang, C.H.; Guo, W.D.; Chen, Y.M.; Lin, L.Y. Numerical simulation of large wave heights from super Typhoon Nepartak (2016) in the Eastern waters of Taiwan. *J. Mar. Sci. Eng.* **2020**, *8*, 217. [[CrossRef](#)]
14. Xu, J.L.; Ma, K.; Nie, Y.L.; Liu, C.Y.; Bi, X.; Shi, W.Q.; Lv, X.Q. Numerical Study on Storm Surge Level Including Astronomical Tide Effect Using Data Assimilation Method. *Atmosphere* **2022**, *14*, 38. [[CrossRef](#)]
15. Xu, J.L.; Nie, Y.L.; Ma, K.; Shi, W.Q.; Lv, X.Q. Assimilation research of wind stress drag coefficient based on the linear expression. *J. Mar. Sci. Eng.* **2021**, *9*, 1135. [[CrossRef](#)]
16. Jing, Y.; Wang, H.; Zhu, P.; Li, Y.B.; Ye, L.; Jiang, L.F.; Wang, A.T. The Sensitivity of Large Eddy Simulations to Grid Resolution in Tropical Cyclone High Wind Area Applications. *Remote Sens.* **2023**, *15*, 3785. [[CrossRef](#)]
17. Kerr, P.C.; Martyc, R.C.; Donahue, A.S.; Hope, M.E.; Westerink, J.J.; Luettich, R.A., Jr.; Kennedy, A.B.; Dietrich, J.C.; Dawson, C.; Westerink, H.J. U.S. IOOS coastal and ocean modeling testbed: Evaluation of tide, wave, and hurricane surge response sensitivities to mesh resolution and friction in the Gulf of Mexico. *J. Geophys. Res. Oceans* **2013**, *118*, 4633–4661. [[CrossRef](#)]
18. Moon, I.J.; Kwon, J.I.; Lee, J.C.; Shim, J.S.; Kang, S.K.; Oh, I.S.; Kwon, S.J. Effect of the surface wind stress parameterization on the storm surge modeling. *Ocean Modell.* **2009**, *29*, 115–127. [[CrossRef](#)]
19. Dukhovskoy, D.S.; Morey, S.L. Simulation of the Hurricane Dennis storm surge and considerations for vertical resolution. *Nat. Hazards* **2011**, *58*, 511–540. [[CrossRef](#)]
20. Mentaschi, L.; Voudoukas, M.I.; Garcia-Sanchez, G.; Fernandez-Montblanc, T.; Roland, A.; Voukouvalas, E.; Federico, I.; Abdolali, A.; Zhang, Y.J.; Feyen, L. A global unstructured, coupled, high-resolution hindcast of waves and storm surge. *Front. Mar. Sci.* **2023**, *10*, 1233679. [[CrossRef](#)]
21. Garzon, J.L.; Ferreira, C.M.; Padilla-Hernandez, R. Evaluation of weather forecast systems for storm surge modeling in the Chesapeake Bay. *Ocean Dyn.* **2018**, *68*, 91–107. [[CrossRef](#)]
22. Makris, C.; Androulidakis, Y.; Karambas, T.; Papadimitriou, A.; Metallinos, A.; Kontos, Y.; Baltikas, V.; Chondros, M.; Krestenitis, Y.; Tsoukala, V.; et al. Integrated modelling of sea-state forecasts for safe navigation and operational management in ports: Application in the Mediterranean Sea. *Appl. Math. Modell.* **2021**, *89*, 1206–1234. [[CrossRef](#)]
23. Mohanty, S.; Nadimpalli, R.; Mohanty, U.C.; Pattanayak, S. Storm surge prediction improvement using high resolution meso-scale model products over the Bay of Bengal. *Nat. Hazard.* **2023**, *120*, 1185–1231. [[CrossRef](#)]
24. Zhao, Y.J.; Greybush, S.J.; Wilson, R.J.; Hoffman, R.N.; Kalnay, E. Impact of assimilation window length on diurnal features in a Mars atmospheric analysis. *Tellus A* **2015**, *67*, 26042. [[CrossRef](#)]
25. Wang, M.J.; Xue, M.; Zhao, K. The impact of T-TREC-retrieved wind and radial velocity data assimilation using EnKF and effects of assimilation window on the analysis and prediction of Typhoon Jangmi (2008). *J. Geophys. Res. Ocean.* **2016**, *121*, 259–277. [[CrossRef](#)]
26. Zheng, X.Y.; Mayerle, R.; Xing, Q.G.; Jaramillo, J.M.F. Adjoint free four-dimensional variational data assimilation for a storm surge model of the German North Sea. *Ocean Dyn.* **2016**, *66*, 1037–1050. [[CrossRef](#)]
27. Kim, H.; Kim, H.M.; Kim, J.; Cho, C.H. Effect of Data Assimilation Parameters on The Optimized Surface CO₂ Flux in Asia. *Asia-Pac. J. Atmos. Sci.* **2018**, *54*, 1–17. [[CrossRef](#)]
28. Dinápoli, M.G.; Ruiz, J.J.; Simionato, C.G.; Berden, G. Improving the short-range forecast of storm surges in the southwestern Atlantic continental shelf using 4DensRF data assimilation. *Q. J. R. Meteorol. Soc.* **2023**, *149*, 2333–2347. [[CrossRef](#)]
29. Khan, M.J.U.; Durand, F.; Bertin, X.; Testut, L.; Krien, Y.; Islam, A.K.M.S.; Pezerat, M.; Hossain, S. Towards an efficient storm surge and inundation forecasting system over the Bengal delta: chasing the Supercyclone Amphan. *Nat. Hazards Earth Syst. Sci.* **2021**, *21*, 2523–2541. [[CrossRef](#)]
30. Madsen, K.S.; Hoyer, J.L.; Fu, W.W.; Donlon, C. Blending of satellite and tide gauge sea level observations and its assimilation in a storm surge model of the North Sea and Baltic Sea. *J. Geophys. Res. Ocean.* **2015**, *120*, 6405–6418. [[CrossRef](#)]
31. Fan, L.L.; Liu, M.M.; Chen, H.B.; Lv, X.Q. Numerical study on the spatially varying drag coefficient in simulation of storm surges employing the adjoint method. *J. Oceanol. Limnol.* **2011**, *29*, 702–717. [[CrossRef](#)]
32. Zhang, J.C.; Lu, X.Q.; Wang, P.; Wang, Y.P. Study on linear and nonlinear bottom friction parameterizations for regional tidal models using data assimilation. *Cont. Shelf Res.* **2011**, *31*, 555–573. [[CrossRef](#)]
33. Li, Y.N.; Peng, S.Q.; Yan, J.; Xie, L.A. On improving storm surge forecasting using an adjoint optimal technique. *Ocean Model.* **2013**, *72*, 185–197. [[CrossRef](#)]
34. Zheng, X.Y.; Mayerle, R.; Wang, Y.B.; Zhang, H. Study of the wind drag coefficient during the storm Xaver in the German Bight using data assimilation. *Dynam. Atmos. Ocean.* **2018**, *83*, 64–74. [[CrossRef](#)]
35. Flowerdew, J.; Horsburgh, K.; Wilson, C.; Mylne, K. Development and evaluation of an ensemble forecasting system for coastal storm surges. *R. Meteorol. Soc.* **2010**, *136*, 1444–1456. [[CrossRef](#)]
36. Xu, J.L.; Zhang, Y.H.; Lv, X.Q.; Liu, Q. Inversion of wind stress drag coefficient in simulating storm surges by means of regularization technique. *Int. J. Environ. Res. Public Health* **2019**, *16*, 3591. [[CrossRef](#)] [[PubMed](#)]
37. He, Y.J.; Lu, X.Q.; Qiu, Z.F.; Zhao, J.P. Shallow water tidal constituents in the Bohai Sea and the Yellow Sea from a numerical adjoint model with TOPEX/POSEIDON altimeter data. *Cont. Shelf Res.* **2004**, *24*, 1521–1529. [[CrossRef](#)]
38. Jelesnianski, C.P. A numerical calculation of storm tides included by a tropical storm impinging on a continental shelf. *Mon. Weather Rev.* **1965**, *93*, 343–358. [[CrossRef](#)]
39. Wu, J. Wind-stress coefficients over sea surface from breeze to hurricane. *J. Geophys. Res. Ocean.* **1982**, *87*, 9704–9706. [[CrossRef](#)]

40. Jeremy, A.; Ingela, P. Quantifying Colocalization by Correlation: The Pearson Correlation Coefficient is Superior to the Mander's Overlap Coefficient. *Cytom. Part A* **2010**, *77*, 733–742.
41. Feng, Y.; Dimitris, M.; Xue, H.J.; Zhang, H.; Carroll, D.; Du, Y.; Wu, H. Improved representation of river runoff in Estimating the Circulation and Climate of the Ocean Version 4 (ECCOV4) simulations: Implementation, evaluation, and impacts to coastal plume regions. *Geosci. Model Dev.* **2021**, *14*, 1801–1819. [[CrossRef](#)]

Disclaimer/Publisher's Note: The statements, opinions and data contained in all publications are solely those of the individual author(s) and contributor(s) and not of MDPI and/or the editor(s). MDPI and/or the editor(s) disclaim responsibility for any injury to people or property resulting from any ideas, methods, instructions or products referred to in the content.